Experimental study of the spectroscopic factors of $^{90-97}$Zr

L. Gan,[1,2] H. B. Sun,[1] Z. H. Li,[3,*] Y. J. Li,[3] J. Su,[3] B. Guo,[3] S. Q. Yan,[3] Y. B. Wang,[3] S. Zeng,[3] Z. Y. Han,[3] X. Y. Li,[3] D. H. Li,[3] T. L. Ma,[3] Y. P. Shen,[3] Y. Su,[3] E. T. Li,[1] S. P. Hu,[1] and W. P. Liu[3]

[1]*College of Physics and Energy, Shenzhen University, Shenzhen 518060, China*

[2]*Key Laboratory of Optoelectronic Devices and Systems of Ministry of Education and Guangdong Province, College of Optoelectronic Engineering, Shenzhen University, Shenzhen 518060, China*

[3]*China Institute of Atomic Energy, P.O. Box 275(10), Beijing 102413, China*

(Received 6 December 2017; revised manuscript received 29 May 2018; published 22 June 2018)

Several zirconium isotopes are in the path of slow neutron capture (s) process, and the direct components of (n,γ) reactions can be derived from their neutron spectroscopic factors. In the present work, the angular distributions of (^{12}C,^{13}C) and (^{13}C,^{12}C) reactions on targets ^{90,92,94,96}Zr were obtained using the high-precision Q3D magnetic spectrograph at the Beijing HI-13 tandem accelerator in China Institute of Atomic Energy. The distorted-wave Born approximation calculations were performed to extract the spectroscopic factors, using three different sets of Woods-Saxon potential parameters for these heavy-ion systems. The neutron spectroscopic factors for the ground state of $^{90-97}$Zr have been obtained and compared with other experimental data.

DOI: 10.1103/PhysRevC.97.064614

I. INTRODUCTION

The elements heavier than the iron group are mainly produced by two types of neutron capture reactions: the rapid (r-) and the slow (s-)neutron capture processes, with the different corresponding time scales [1–5]. The time scale of s process is long enough to make all possible β^- decays to take place, which allow the s nuclei to occupy the β-stability valley region. Of various nuclear processes within the heavy element nucleosynthesis, the s process is perhaps the easiest one to study, because many relatively minor abundance heavy elements, such as Y, Zr, Ba, and La are observably affected by s process, and the abundance changes can be observed by spectroscopic techniques [6]. In order to understand the heavy elements production in the universe, accurate neutron cross section data in the celestial environment are of primary importance [7,8].

Zr isotopes, which occupy the intersection of the weak (from Fe to Zr) and main (from Zr to Pb/Bi) s process, have received great attention, and the neutron capture reactions by Zr isotopes are particularly significant [9]. For Zr isotopes, their neutron number is at or close to the magic number of 50, their neutron capture cross sections are relatively low [4,5,7–11]. So far, experimental data for the (n,γ) cross section of Zr isotopes are extremely scarce, especially for the unstable isotopes, such as ^{89}Zr($t_{1/2} = 3.3d$), ^{93}Zr ($t_{1/2} = 1.5 \times 10^6 y$) and ^{95}Zr($t_{1/2} = 64.0d$). The abundances of the Zr isotopes are used to extract valuable information about various constraints regarding the astrophysical medium, including the neutron flux density and temperature, so that the neutron capture reactions rates of Zr isotopes should to be determined with high accuracy. For an example, the ^{93}Zr$(n,\gamma)^{94}$Zr reaction rates should be measured with an accuracy of 3%–5% [9]. The direct components of (n,γ) reactions for Zr isotopes can contribute about 10% to the total reaction rates according to the evaluated data from the National Nuclear Data Center. In terms of ^{89}Zr$(n,\gamma)^{90}$Zr, the direct neutron capture reaction rate takes up about 13% of the total reaction rate. The value is much larger than the demand accuracy of 5%, and it is meaningful to study the direct components of neutron capture reaction accurately with various experiments.

The spectroscopic factor is defined as the overlap between the initial and the final states in the reaction channels. It describes the single-particle structure of nuclei in the shell model, and is the basic element for the understanding of the nuclear structure [12–15], and can be used to estimate the direct component of the (n,γ) cross section. The values of the spectroscopic factor can be obtained by comparing the experimental cross sections with the predicted cross sections from a reaction model. The most commonly used model is the distorted-wave Born approximation (DWBA) theory. Over the past half century, considerable effort has been devoted to the experimental measurements of the neutron spectroscopic factors concerning zirconium isotopes [16–46], including (d,p), (p,d), $(\alpha,^3\mathrm{He})$, and $(^3\mathrm{He},\alpha)$. However, the published spectroscopic factors fail to agree with each other. Especially for ^{90}Zr, the published neutron spectroscopic factors are found to vary from 3.4–10.0, and such large difference may cause more than 20% uncertainty to the total reaction rate of ^{89}Zr$(n,\gamma)^{90}$Zr. The shortage of the previous works mainly lies in two aspects: the large experimental errors (such as Ref. [23] 20%, Ref. [32] 30%–40%) and the ignorance of the influence of the optical potential, which may bring large uncertainties to the spectroscopic factors. In order to improve these defects, a more accurate experiment and more meticulous error analysis should be carried out.

*zhli@ciae.ac.cn

TABLE I. Isotopic composition of targets (%).

Mass number	$^{90}ZrO_2$	$^{92}ZrO_2$	$^{94}ZrO_2$	$^{96}ZrO_2$
90	99.4	0.97	0.7	7.19
91	0.3	0.51	0.2	1.46
92	0.2	98.06	0.4	2.31
94	0.1	0.41	98.6	0.89
96	0.04	0.05	0.1	85.15

In this work, the neutron spectroscopic factors of $^{90-97}$Zr were extracted through angular distribution of (^{12}C,^{13}C) and (^{13}C,^{12}C) reactions on targets ^{90,92,94,96}Zr. The experiments were performed with the Q3D magnetic spectrograph at the HI-13 tandem accelerator in China Institute of Atomic Energy (CIAE), Beijing. The Q3D magnetic spectrograph has a high-energy resolution of about 0.02%, and the angular distributions can be measured with high precision. The neutron spectroscopic factors of $^{90-97}$Zr were then extracted accurately by means of DWBA analysis.

II. EXPERIMENTS

Enriched targets of $^{90,92,94,96}ZrO_2$ were bombarded with 66.0 MeV ^{12}C and 64.0 MeV ^{13}C beams, respectively. The abundance of Zr isotopes was shown in Table I.

The angular distributions of ^{12,13}C+Zr elastic scattering, and (^{12}C,^{13}C) and (^{13}C,^{12}C) neutron transfer reactions were measured. The experimental setup is shown in Fig. 1. The ^{12}C and ^{13}C beams from the accelerator impinged on the carbon-supported zirconium enriched isotope targets of ZrO_2. The thicknesses of the $^{90,92,94,96}ZrO_2$ were 32.9 ± 2.5 μg/cm^2,30.0 ± 2.2 μg/cm^2,41.0 ± 2.9 μg/cm^2, and 34.4 ± 2.3 μg/cm^2, respectively, which were calibrated by normalizing the elastic scattering cross sections of front angles to the Rutherford scattering cross sections. The diameter of the target chamber is 479 mm, and the accepted solid angle of Q3D magnetic spectrometer was set to be 0.34 ± 0.01 msr for excellent angular resolution. A movable Faraday cup was placed behind the target to monitor the beam intensity. A ΔE-E detector telescopic system was set at about 23° downstream of the reaction target for the cross check of the beam intensity. The reaction products were separated by Q3D and then measured by a 50 mm × 50 mm two-dimensional position-sensitive silicon detector (PSSD) at the focal plane. The high momentum resolution of Q3D and the position-energy information about PSSD enable us to identify the object ions from other reaction channels.

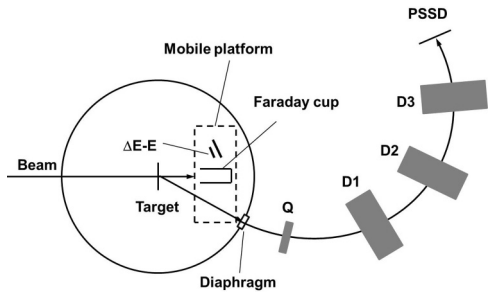

FIG. 1. Experimental setup.

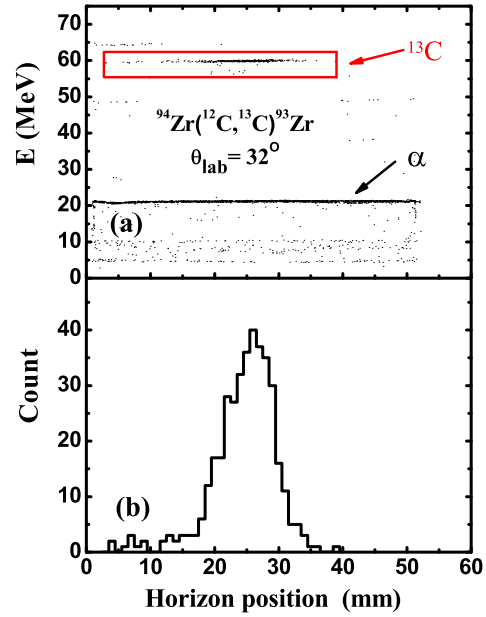

FIG. 2. (a) The two-dimensional spectrum of kinetic energy versus the horizon position and (b) the horizon position spectrum of object ions for ^{94}Zr(^{12}C,^{13}C)^{93}Zr at 32°.

The typical two-dimensional spectrum of kinetic energy versus the horizon position for ^{94}Zr(^{12}C,^{13}C)^{93}Zr reaction at 32° is shown in Fig. 2(a). It can be seen that the object ions from the reactions can be clearly identified via the energy and position information, so that the number of object ions can be counted accurately through the position spectrum of object ions, as shown in Fig. 2(b).

III. DWBA ANALYSIS

For ^{90,92,94,96}Zr(^{12}C,^{13}C) and (^{13}C,^{12}C) one-neutron transfer reactions, the angular distributions are peaked around 30°. The shapes of the angular distributions show a slight different as can be seen in Figs. 5 and 6.

The experimental cross sections were analyzed with DWBA calculations. This procedure supports the extraction of the spectroscopic factors by taking the ratios of the experimental cross sections to the predicted cross sections. The equation can be expressed as:

$$\frac{d\sigma_{\rm exp}}{d\Omega} = S_{^{13}\rm C} S_{\rm Zr} \frac{d\sigma_{\rm DWBA}}{d\Omega}, \quad (1)$$

where the $d\sigma_{\rm exp}/d\Omega$ and $d\sigma_{\rm DWBA}/d\Omega$ are the experimental and DWBA theory differential cross sections of transfer reaction, respectively. The $S_{^{13}\rm C}$ and $S_{\rm Zr}$ denote the neutron spectroscopic factors for the ground state of $^{13}\rm C = {}^{12}C \otimes n$ and $^{A+1}\rm Zr = {}^{A}Zr \otimes n$, respectively. $S_{^{13}C} = 0.65 \pm 0.06$ was adopted from the result given by Al-Abdullah *et al.* [47]. The geometrical parameters of the single-particle bound state were set to be $r_0 = 1.25$ fm and $a_0 = 0.65$ fm.

TABLE II. Optical potential parameters of ^{12,13}C+Zr.

System		V (MeV)	r_V (fm)	a_V (fm)	W (MeV)	r_W (fm)	a_W (fm)	r_C (fm)
^{12}C + ^{90,91}Zr	set1	63.9	1.23	0.52	35.0	1.15	0.56	1.0
	set2	98.0	1.21	0.50	29.5	1.16	0.57	1.0
	set3	33.7	1.28	0.54	31.9	1.28	0.37	1.0
^{13}C + ^{89,90}Zr	set1	63.0	1.23	0.52	35.0	1.15	0.56	1.0
	set2	99.2	1.17	0.57	29.6	1.17	0.54	1.0
	set3	34.5	1.27	0.58	34.9	1.29	0.33	1.0
^{12}C + ^{92,93}Zr	set1	63.6	1.23	0.52	35.0	1.15	0.56	1.0
	set2	83.8	1.21	0.50	31.8	1.14	0.71	1.0
	set3	29.8	1.30	0.51	28.9	1.25	0.51	1.0
^{13}C + ^{91,92}Zr	set1	62.6	1.23	0.52	35.0	1.15	0.56	1.0
	set2	90.6	1.22	0.50	31.8	1.14	0.66	1.0
	set3	32.6	1.31	0.51	31.3	1.26	0.44	1.0
^{12}C + ^{94,95}Zr	set1	63.2	1.23	0.52	35.0	1.15	0.56	1.0
	set2	99.5	1.18	0.55	38.4	1.17	0.57	1.0
	set3	32.3	1.29	0.50	34.9	1.11	0.66	1.0
^{13}C + ^{93,94}Zr	set1	62.3	1.23	0.52	35.0	1.15	0.56	1.0
	set2	100.1	1.16	0.58	33.9	1.18	0.56	1.0
	set3	34.5	1.25	0.63	35.4	1.27	0.38	1.0
^{12}C + ^{96,97}Zr	set1	62.9	1.23	0.52	35.0	1.15	0.56	1.0
	set2	100.4	1.18	0.55	30.3	1.17	0.53	1.0
	set3	32.4	1.26	0.6	27.4	1.28	0.38	1.0
^{13}C + ^{95,96}Zr	set1	61.9	1.23	0.52	35.0	1.15	0.56	1.0
	set2	98.7	1.17	0.59	29.4	1.17	0.57	1.0
	set3	33.3	1.26	0.63	29.0	1.28	0.40	1.0

To extract spectroscopic information, the computer code FRESCO [48] and a volume Woods-Saxon form for the real and imaginary potential were used. In order to analyze the influence of heavy-ion interaction potential, three sets of optical potential parameters were adopted in the DWBA calculations, as shown in Table II. Set1 was taken from Ref. [49], and no attempt was made to fit the reaction data by varying these parameters. Set2 and Set3 were obtained by fitting the elastic scattering angular distributions, and the optical parameters of ^{12,13}C + ^{89,91,93,95,97}Zr were substituted with the adjacent Zr isotopes. As shown in Figs. 3 and 4, the elastic scattering angular distributions of ^{12,13}C+Zr were calculated with these three optical parameter sets. It can be seen that the experimental data were well reproduced with the optical potential parameters.

DWBA calculations were performed for the ground state of $^{90\sim97}$Zr by using the parameters listed in Table II. The

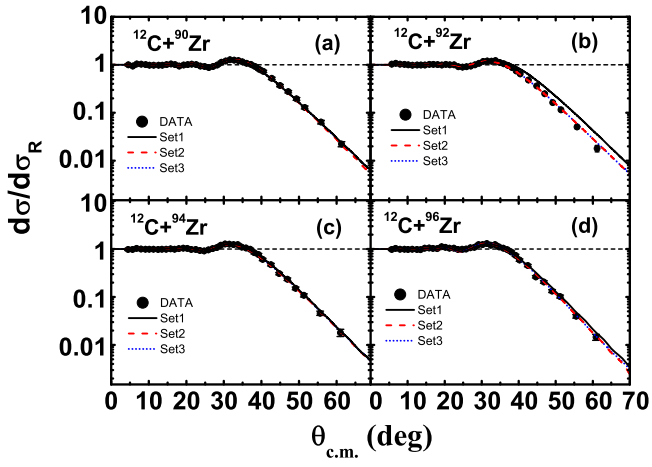

FIG. 3. The angular distributions of differential cross sections of ^{12}C + ^{90,92,94,96}Zr. The solid curves are calculated by Set1, the red dashes and blue short dashes represent the results of Set2 and Set3, while dots are experimental distributions.

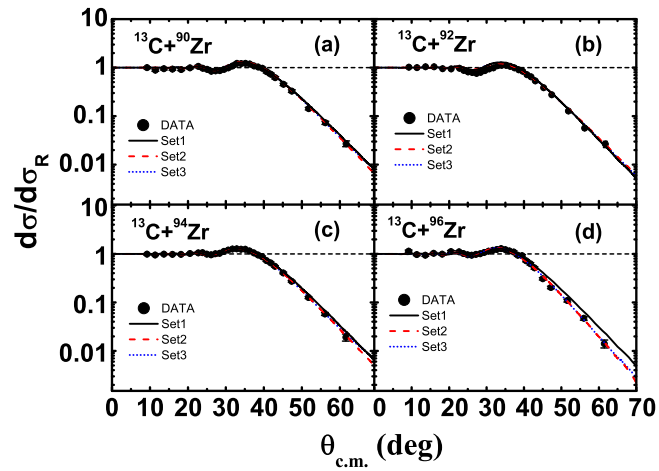

FIG. 4. The angular distributions of differential cross sections of ^{13}C + ^{90,92,94,96}Zr.

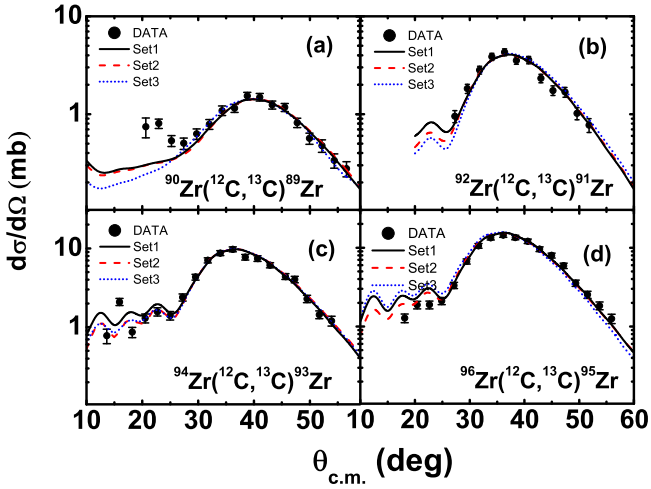

FIG. 5. The angular distributions of differential cross sections of ^{90,92,94,96}Zr(^{12}C,^{13}C).

calculated results are shown in Figs. 5 and 6 as three kinds of different curves. It can be seen that at the peaks of these angular distributions, all the theoretical curves can describe the experimental data successfully. However, the differential cross sections below 30° agreed not well due to the influence of other reaction mechanisms. The neutron spectroscopic factors from the present investigations of the (^{12}C, ^{13}C) and (^{13}C, ^{12}C) reactions on ^{90,92,94,96}Zr are summarized in Table III. It is obvious that the spectroscopic factors extracted by three sets of optical parameters were extremely close to each other. The average values were considered as the result of the present work. The uncertainties of the spectroscopic factors consist of the experimental errors (statistics errors and the nonuniformity of the target thickness, about 10%), the influence of the optical parameters (from 1%–12%) and the error of $S_{^{13}C}$ (9%).

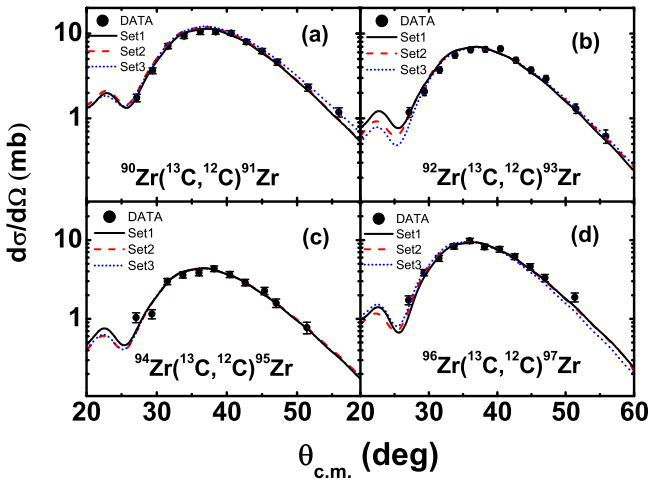

FIG. 6. The angular distributions of differential cross sections of ^{90,92,94,96}Zr(^{13}C,^{12}C).

TABLE III. The results of neutron spectroscopic factors of $^{90-97}$Zr.

Isotopes	Set1	Set2	Set3	Average
^{90}Zr	7.51 ± 1.02	7.53 ± 1.03	7.26 ± 0.99	7.43 ± 1.02
^{91}Zr	0.82 ± 0.12	0.86 ± 0.10	0.83 ± 0.10	0.84 ± 0.11
^{92}Zr	1.26 ± 0.16	1.67 ± 0.22	1.51 ± 0.20	1.48 ± 0.26
^{93}Zr	0.45 ± 0.06	0.58 ± 0.07	0.54 ± 0.06	0.52 ± 0.08
^{94}Zr	2.89 ± 0.40	2.88 ± 0.40	2.74 ± 0.33	2.84 ± 0.38
^{95}Zr	0.27 ± 0.04	0.30 ± 0.04	0.28 ± 0.04	0.28 ± 0.04
^{96}Zr	3.94 ± 0.59	3.81 ± 0.57	3.64 ± 0.51	3.80 ± 0.57
^{97}Zr	0.74 ± 0.10	0.75 ± 0.11	0.73 ± 0.10	0.74 ± 0.10

TABLE IV. Comparison of the neutron spectroscopic factors of ^{90}Zr.

Ref.	$S_{^{90}Zr}$	Reaction	E_{lab} (MeV)
[16]	9.6 ± 1.3	(p,d)	31
[17]	6.1 ± 0.6	(pol p,d)	22
[18]	9.5 ± 1.4	(p,d)	55
[19]	4.8 ± 0.6	(p,d)	65
[20]	5.1 ± 0.8	(p,d)	120
[21]	3.9 ± 0.4	(pol p,d)	65
[22]	8.9	(pol p,d)	90
[23]	9.6 ± 1.9	(pol p,d)	90
[24]	7.7 ± 0.5	(d,t)	21.4
[25]	10.0 ± 2.0	(^{3}He,α)	18
[26]	3.41	(^{3}He,α)	25
[27]	8.0 ± 0.8	(^{3}He,α)	39
[28]	9.7 ±1.94	(^{3}He,α)	18
[29]	9.1 ± 0.9	(^{3}He,α)	97.3
Present	7.43 ± 1.02	(^{12}C,^{13}C)	66

TABLE V. Comparison of the neutron spectroscopic factors of ^{91}Zr.

Ref.	$S_{^{91}Zr}$	Reaction	E_{lab} (MeV)
[16]	0.98 ± 0.10	(p,d)	31
[26]	0.67	(^{3}He,α)	25
[30]	0.94	(^{3}He,α)	24
[31]	0.98 ± 0.15	(α,^{3}He)	65.9
[31]	1.04 ± 0.16	(d,p)	33
[32]	0.89 ± 0.09	(d,p)	15
[33]	0.95 ± 0.14	(d,p)	7.5
[34]	0.75 ± 0.08	(d,p)	15.9
[34]	1.09	(pol d,p)	11.1
[35]	0.69 ± 0.07	(pol d,p)	56
[36]	0.98	(^{13}C,^{12}C)	28-33.5
[37]	1.0	(^{16}O,^{15}O)	104
Present	0.84 ± 0.11	(^{13}C,^{12}C)	66

TABLE VI. Comparison of the neutron spectroscopic factors of ^{92}Zr.

Ref.	$S_{^{92}\mathrm{Zr}}$	Reaction	E_{lab} (MeV)
[16]	1.86 ± 0.33	(p,d)	31
[34]	1.18 ± 0.12	(p,d)	22
[38]	1.43 ± 0.29	(pol p,d)	22
[26]	0.86	(^{3}He,α)	25
[27]	1.46 ± 0.15	(^{3}He,α)	39
[31]	1.14 ± 0.17	(α,^{3}He)	66
[31]	1.89 ± 0.28	(d,p)	33
[32]	1.44 ± 0.14	(d,p)	15
[39]	1.21 ± 0.18	(d,p)	12
[40]	1.08 ± 0.22	(d,p)	12
[41]	1.56 ± 0.31	(pol d,p)	33
Present	1.48 ± 0.26	(^{12}C,^{13}C)	66

TABLE VII. Comparison of the neutron spectroscopic factors of ^{93}Zr.

Ref.	$S_{^{93}\mathrm{Zr}}$	Reaction	E_{lab} (MeV)
[32]	0.54 ± 0.05	(d,p)	15
[42]	0.64 ± 0.10	(d,p)	33
[42]	0.48 ± 0.07	(^{3}He,α)	65.7
Present	0.52 ± 0.08	(^{13}C,^{12}C)	66

TABLE VIII. Comparison of the neutron spectroscopic factors of ^{94}Zr.

Ref.	$S_{^{94}\mathrm{Zr}}$	Reaction	E_{lab} (MeV)
[21]	2.18 ± 0.22	(pol p,d)	65
[43]	2.5 ± 0.25	(p,d)	19.4
[26]	2.16	(^{3}He,α)	25
[27]	2.61 ± 0.26	(^{3}He,α)	39
[32]	3.41 ± 0.34	(d,t)	15
Present	2.84 ± 0.38	(^{12}C,^{13}C)	66

TABLE IX. Comparison of the neutron spectroscopic factors of ^{95}Zr.

Ref.	$S_{^{95}\mathrm{Zr}}$	Reaction	E_{lab} (MeV)
[32]	0.30 ± 0.09	(d,p)	15
[42]	0.37 ± 0.06	(d,p)	33
[44]	0.32 ± 0.01	(d,p)	15.5
[42]	0.36 ± 0.05	(^{3}He,α)	65.7
Present	0.28 ± 0.04	(^{13}C,^{12}C)	66

TABLE X. Comparison of the neutron spectroscopic factors of ^{96}Zr.

Ref.	$S_{^{96}\mathrm{Zr}}$	Reaction	E_{lab} (MeV)
[32]	5.75 ± 0.58	(d,t)	15
[45]	4.41	(p,d)	19.4
[27]	4.5 ± 0.5	(^{3}He,α)	39
Present	3.8 ± 0.57	(^{12}C,^{13}C)	66

TABLE XI. Comparison of the neutron spectroscopic factors of ^{97}Zr.

Ref.	$S_{^{97}\mathrm{Zr}}$	Reaction	E_{lab} (MeV)
[32]	0.98 ± 0.39	(d,p)	15
[42]	1.20 ± 0.18	(d,p)	33
[46]	1.06 ± 0.11	(pol d,p)	12
[42]	1.02 ± 0.15	(α,^{3}He)	65.7
Present	0.74 ± 0.10	(^{13}C,^{12}C)	66

The comparison of neutron spectroscopic factors obtained in the present work and that from the previous works was shown in Tables IV–XI and displayed in Figs. 7 and 8. It is evident that our results of $^{90-97}$Zr are in accordance with the average values.

IV. CONCLUSIONS

Zr isotopes are in the path of the s process, their neutron capture reactions are very important in the heavy elements synthesis and should to be determined with a high accuracy of about 5%. The direct components of neutron capture reaction take up about 10% in the total capture cross sections and thus are worth measuring accurately with various experiments.

In the present work, the angular distribution of (^{12}C,^{13}C) and (^{13}C,^{12}C) on the Zr isotopes targets are measured with the high-resolution Q3D magnetic spectrograph. The neutron spectroscopic factors of $^{90-97}$Zr are extracted by comparing the differential cross sections of experimental and DWBA calculations. The current spectroscopic factors are in very significant good agreement with the average values of the previous works. It is worth noting that the data measured in this work have better precision than most of the previous works, and the theoretical calculations can reproduce the measured

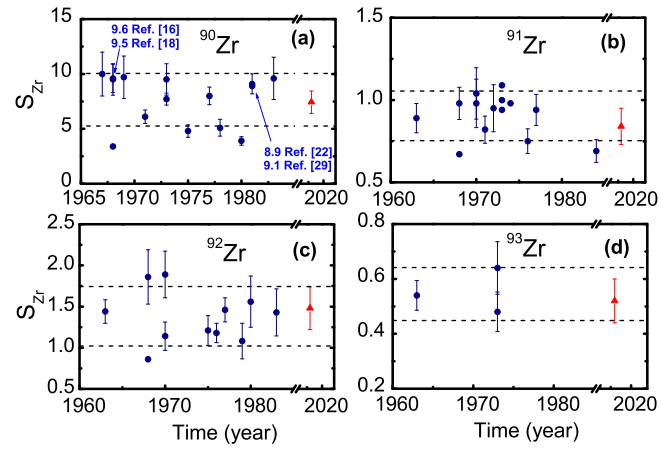

FIG. 7. The neutron spectroscopic factors of $^{90-93}$Zr. The blue dots are the spectroscopic factors from the references, and the red triangle represent our result. The dotted lines show the average value region.

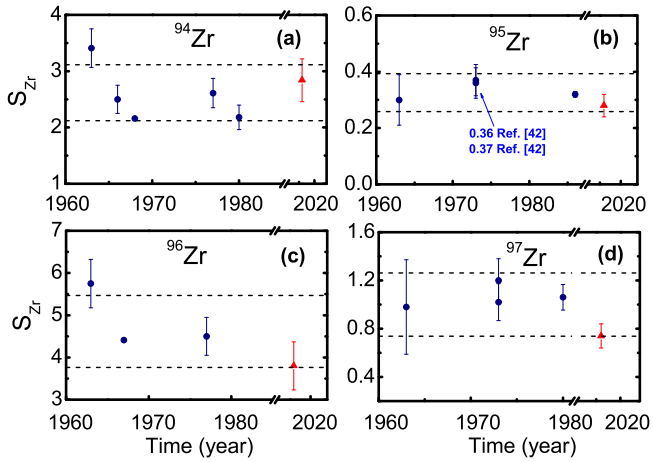

FIG. 8. The neutron spectroscopic factors of $^{94-97}$Zr.

angular distributions very well. The influence of the optical potential has been also considered by adopting three parameter sets.

ACKNOWLEDGMENTS

This work was performed with the support of the National Natural Science Foundation of China under Grants No. 11375269, No. 11490563, No. 11575118 and No. 11605114, the 973 program of China under Grant No. 2013CB834406, the National key Research and Development Program of China under Grant No. 2016YFA0400502, the National Key Scientific Instrument and Equipment Development Projects of China (2017YFF0106501), as well as the National Natural Science Foundation of Guangdong Province, China (2016A030310042).

[1] E. M. Burbidge, G. R. Burbidge, W. A. Fowler *et al.*, Rev. Mod. Phys. **29**, 547 (1957).
[2] A. G. W. Cameron, Pub. Astron. Soc. Pac. **69**, 201 (1957).
[3] M. Arnould and K. Takahashi, Rep. Prog. Phys. **62**, 395 (1999).
[4] S. Dutta, G. Gangopadhyay, and A. Bhattacharyya, Phys. Rev. C **94**, 024604 (2016).
[5] M. Guttormsen, S. Goriely, A. C. Larsen *et al.*, Phys. Rev. C **96**, 024313 (2017).
[6] G. Wallerstein, I. Iben, P. Parker *et al.*, Rev. Mod. Phys. **69**, 995 (1997).
[7] F. Käppeler, Prog. Part. Nucl. Phys. **43**, 419 (1999).
[8] N. Colonna, U. Abbondanno, G. Aerts *et al.*, Appl. Radiat. Isot. **68**, 643 (2010).
[9] G. Tagliente, P. M. Milazzo, K. Fujii *et al.*, Phys. Rev. C **87**, 014622 (2013).
[10] W. Hauser and H. Feshbach, Phys. Rev. **87**, 366 (1952).
[11] M. Lugaro, F. Herwig, J. C. Lattanzio, R. Gallino, and O. Straniero, Astrophys. J. **586**, 1305 (2003).
[12] M. H. Macfarlane and J. B. French, Rev. Mod. Phys. **32**, 567 (1960).
[13] J. M. Udías, P. Sarriguren, E. Moya de Guerra, E. Garrido, and J. A. Caballero, Phys. Rev. C **48**, 2731 (1993).
[14] J. Lee, M. B. Tsang, and W. G. Lynch, Phys. Rev. C **75**, 064320 (2007).
[15] F. Becka, D. Frekersb, P. von Neumann-Cosel *et al.*, Phys. Lett. B **645**, 128 (2007).
[16] J. B. Ball and C. B. Fulmer, Phys. Rev. **172**, 1199 (1968).
[17] B. Mayer, J. Gosset, J. L. Escudie *et al.*, Nucl. Phys. A **177**, 205 (1971).
[18] H. Taketani, M. Adachi, M. Ogawa *et al.*, Nucl. Phys. A **204**, 385 (1973).
[19] P. G. Roos, S. M. Smith, V. K. C. Cheng *et al.*, Nucl. Phys. A **255**, 187 (1975).
[20] R. E. Anderson, J. J. Kraushaar, J. R. Shepard *et al.*, Nucl. Phys. A **311**, 93 (1978).
[21] K. Hosono, M. Kondo, T. Saito *et al.*, Nucl. Phys. A **343**, 234 (1980).
[22] G. M. Crawley, J. Kasagi, S. Gales, E. Gerlic, D. Friesel, and A. Bacher, Phys. Rev. C **23**, 1818 (1981).
[23] J. Kasagi, G. M. Crawley, E. Kashy, J. Duffy, S. Gales, E. Gerlic, and D. Friesel, Phys. Rev. C **28**, 1065 (1983).
[24] S. Takeda, J. Phys. Soc. Jpn. **34**, 304 (1973).
[25] C. M. Fou, R. W. Zurmühle, and J. M. Joyce, Phys. Rev. **155**, 1248 (1967).
[26] D. E. Rundquist, M. K. Brussel, A. I. Yavin *et al.*, Phys. Rev. **168**, 1296 (1968).
[27] S. Galés, E. Hourani, S. Fortier *et al.*, Nucl. Phys. A **288**, 201 (1977).
[28] G. Bassani and J. Picard, Nucl. Phys. A **131**, 653 (1969).
[29] G. Duhamel, G. Perrin, J. P. Didelez *et al.*, J. Phys. G: Nucl. Phys. **7**, 1415 (1981).
[30] H. Fann, J. Schiffer, and U. Strohbusch, Phys. Lett. B **44**, 19 (1973).
[31] C. R. Bingham and M. L. Halbert, Phys. Rev. C **2**, 2297 (1970).
[32] B. L. Cohen and O. V. Chubinsky, Phys. Rev. **131**, 2184 (1963).
[33] A. Graue, L. Herland, and K. Lervik, Nucl. Phys. A **187**, 141 (1972).
[34] H. Block, L. Hulstman, E. Kaptein *et al.*, Nucl. Phys. A **273**, 142 (1976).
[35] R. D. Rathmell, P. J. Bjorkholm, and W. Haeberli, Nucl. Phys. A **206**, 459 (1973).
[36] G. Gill, R. Gill, and G. Jones, Nucl. Phys. A **224**, 140 (1974).
[37] M. S. Zisman, F. D. Becchetti, B. G. Harvey *et al.*, Phys. Rev. C **8**, 1866 (1973).
[38] Y. Aoki, H. Iida, K. Nagano *et al.*, Nucl. Phys. A **393**, 52 (1983).
[39] S. Ipson, K. McLean, W. Booth *et al.*, Nucl. Phys. A **253**, 189 (1975).
[40] T. Borello-Lewin, H. M. A. Castro, L. B. Horodynski-Matsushigue, and O. Dietzsch, Phys. Rev. C **20**, 2101 (1979).
[41] J. Bieszk, Nucl. Phys. A **339**, 513 (1980).

[42] C. R. Bingham and G. T. Fabian, Phys. Rev. C **7**, 1509 (1973).
[43] M. M. Stautberg and J. J. Kraushaar, Phys. Rev. **151**, 969 (1966).
[44] E. Frota-Pessôa and S. Joffily, Il Nuovo Cimento A (1965-1970) **91**, 370 (1986).
[45] M. M. Stautberg, R. Johnson, J. Kraushaar *et al.*, Nucl. Phys. A **104**, 67 (1967).
[46] D. A. Hennies, Ph.D. thesis, University of Wisconsin, Madison, 1980.
[47] T. Al-Abdullah, F. Carstoiu, X. Chen *et al.*, Phys. Rev. C **81**, 035802 (2010).
[48] I. J. Thompson, Comput. Phys. Rep. **7**, 167 (1988).
[49] L. Gan, Z. H. Li, H. B. Sun *et al.*, Sci. China-Phys. Mech. Astron. **60**, 082013 (2017).